THE UNIVERSITY *of* EDINBURGH

Edinburgh Research Explorer

Quantitative Spatial Mapping of Mixing in Microfluidic Systems

OPEN ACCESS

Quantitative Spatial Mapping of Mixing in Microfluidic Systems**

Steven W. Magennis,[1,2] Emmelyn M. Graham[1,2] and Anita C. Jones[1,2,*]

[1]Collaborative Optical Spectroscopy, Micromanipulation and Imaging Centre (COSMIC), The University of Edinburgh, King's Buildings, Edinburgh EH9 3JZ, UK.

[2]EaStCHEM, School of Chemistry, Joseph Black Building, University of Edinburgh, West Mains Road, Edinburgh, EH9 3JJ, UK.

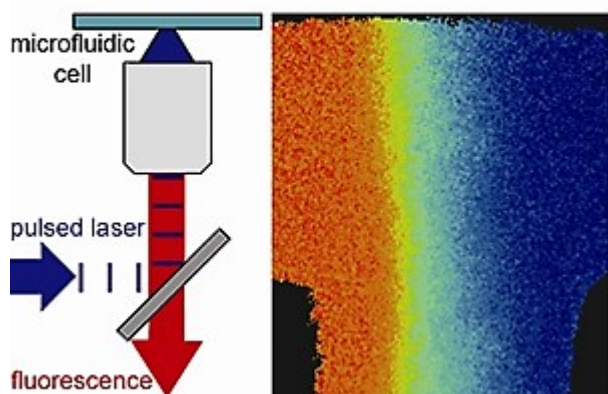[*]Corresponding author; e-mail: a.c.jones@ed.ac.uk, fax: (+44) 131 650 4743

Graphical abstract:

Abstract

The problem of miniaturizing the mixing process is a barrier to the advance of microfluidic technology. Fluorescence lifetime imaging is a powerful technique for the quantitative mapping of mixing in microfluidic systems, providing information essential to the design and evaluation of next-generation devices.

Main text

Microfluidics promises to revolutionize chemical analysis,[1,2] synthesis[3-5] and biotechnology,[6] by combining processes such as mixing, separation, reaction and detection in a single device. These systems function as "labs-on-a-chip",[7] creating a technology that is low-cost, high-throughput, miniaturized, and automated. Many benefits of microfluidics arise from the reduction in size, but miniaturization results in a fundamental change in flow characteristics. Turbulent flow predominates at the macroscale, while fluids flow in a laminar fashion at the microscale, without the random mixing that is characteristic of turbulence.[8] These laminar flow conditions mean that multiple fluid streams tend to flow in parallel through microchannels, mixing only by diffusion across their interfaces.[9] Whilst laminar flow behavior has been exploited to good effect in microanalytical systems, many emerging applications of microfluidic devices require rapid and efficient mixing.

Miniaturizing the mixing process has been identified as a major bottleneck in the performance and development of microfluidic devices.[10] In labs-on-a-chip, the purpose of mixing is generally to bring together solute species from two (or more) flows. In the laminar flow regime, mixing occurs slowly by diffusion of solute (and solvent) molecules across the flow boundary. To achieve rapid mixing, laminar flow must be disrupted to give chaotic mixing, in which there is bulk transfer of fluid (solvent carrying solute) between the flows.

Micromixers can be either passive (static) or active devices. Passive micromixing strategies frequently rely on diffusional mixing, using multilamination, or flow-splitting, techniques to reduce the mixing equilibration time.[11] To increase the mixing rate beyond that limited by diffusion, passive mixers that induce lateral transport of fluid between streams have been devised.[12, 13] Active micromixers use miniature stirrers or external fields to chaotically intersperse fluid flows. In spite of the increasing attention paid to the mixing problem, devices are still designed by trial-and-error methods.[12] It is essential, therefore, that techniques capable of visualizing fluid composition with high quantitation and spatial resolution are found. This will allow testing of prototype devices, and will provide essential experimental data to guide development of theoretical models and validate computational simulations. Computational fluid dynamics models have proved useful in preliminary mixer designs, but a rigorous understanding of the fundamental principles of microfluidics would lead to the development of better models for complex mixing devices.[15]

The most common methods for visualizing flow and mixing efficiency are fluorescence intensity imaging[9,10,13,16] and transmitted light microscopy using colored dyes, pH indicators, and colored reaction products.[8,15,17] These techniques are relatively cheap, easy to set up, and, in the case of fluorescence imaging, provide excellent contrast. Unfortunately, the ability of these intensity-based techniques to provide a quantitative picture of fluid composition in microfluidic systems is severely compromised by their sensitivity to variations in the optical path, instability of the light source, scattering, uncertainty in the dye concentration, and photobleaching effects.[18]

Here we describe a superior approach to the imaging of microfluidic systems using fluorescence lifetime imaging microscopy (FLIM). This technique involves spatially resolving the fluorescence lifetime of a fluorescent dye, rather than the intensity, and overcomes all of the aforementioned problems of intensity-based methods because the lifetime is independent of the number of fluorescing molecules. To date, the use of FLIM has been restricted to the imaging of biological systems.[19-21] We now demonstrate that FLIM enables spatially-resolved quantification of fluid mixing in microfluidic devices.

Solutions of the fluorescent dye 1,8-anilinonaphthalene sulfonate (ANS) in pure methanol and a water-methanol mixture (1:1 molar ratio, which corresponds to 30.8% water v/v) were pumped into a microchannel flow cell, meeting head-on at the top of a T-junction, as illustrated in the schematic in Figure 1a. The flow channels had a depth of 200 μm and width of 400 μm and the flow rates were varied from 10-75 μL/min. These dimensions and flow rates correspond to Reynolds numbers < 10, such that the fluids are in the laminar flow regime.[17]
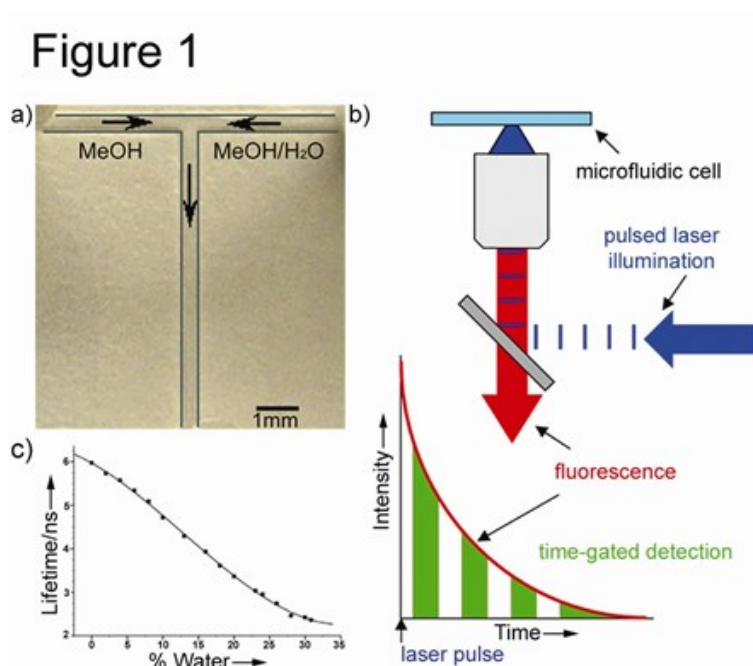

Figure 1. (a) Photograph of the microfluidic flow cell. Arrows indicate the direction of flow. The channel edges have been highlighted for clarity. (b) Schematic of fluorescence lifetime imaging microscopy (FLIM).

(c) Calibration curve showing the dependence of ANS fluorescence lifetime upon the methanol/water composition. The equation $Y =5.97258-0.09267 X-0.00382 X^2+9.82168E-5 X^3$, where Y is the lifetime in ns, and X is the concentration of water in the water-methanol mixture (% v/v) gave a good fit to the data. The concentration of ANS was 10^{-3} M. Lifetimes were measured by TCSPC. The decays and fitted data are shown in Figure S1 and Table S1, respectively.

Fluorescence lifetime images were obtained using widefield illumination of the microfluidic cell with an ultrafast pulsed laser, and collection of the resultant fluorescence in a short time window at a particular delay time after the laser pulse using a gated intensified CCD camera. A series of images is acquired by varying the delay time between the detection window and the laser pulse, thereby sampling the entire fluorescence decay of the ANS probe (Figure 1b); the data from each pixel is then fitted to a single exponential decay. ANS was chosen as the dye because its fluorescence lifetime is extremely sensitive to the composition of water-methanol mixtures, showing a near-linear variation from 250 ps in pure water to 6 ns in pure methanol.[22] The calibration curve in Figure 1c, which quantifies the dependence of the lifetime of ANS upon the water/methanol composition, was determined by time-correlated single photon counting (Figure S1 and Table S1). ANS displays a single exponential decay at all compositions of water and methanol, making it an ideal, unambiguous probe of solvent composition.

The effectiveness of the time-resolved technique is demonstrated in Figure 2, which compares intensity and lifetime images for two regions of the flow cell during a typical experiment. The intensity and FLIM images, which are displayed using the same pseudocolor scale, are noticeably different. The intensity images (Figure 2a) show large, irregular variations in intensity across the field of view, with the highest intensity regions located near the input of the solution of ANS in methanol. The FLIM images give a clear and unambiguous picture of the liquid composition (Figure 2b). These images show smooth transitions from long to short lifetime (left to right), across a clearly defined mixing region. By using the calibration curve in Figure 1c, the composition at each point in the FLIM image can be directly read off. In principle, there should be a clear correlation between the intensity images and the lifetime images; the longer the fluorescence lifetime, the higher the quantum yield and hence the higher the fluorescence intensity (given that the ANS concentration is constant). In practice, however, no such correlation is apparent and it is clear that the intensity-based images are strongly distorted by variation of the illuminating field, the collection efficiency and the other variables previously mentioned. The microfluidic flow cell used in this study is of a simple design, and it is likely that intensity-based imaging will be even more prone to optical artifacts in complex devices. FLIM, on the other hand, faithfully reports the fluid composition, as the lifetime is governed solely by the solvent environment of the ANS probe, and is immune to other undesirable effects.
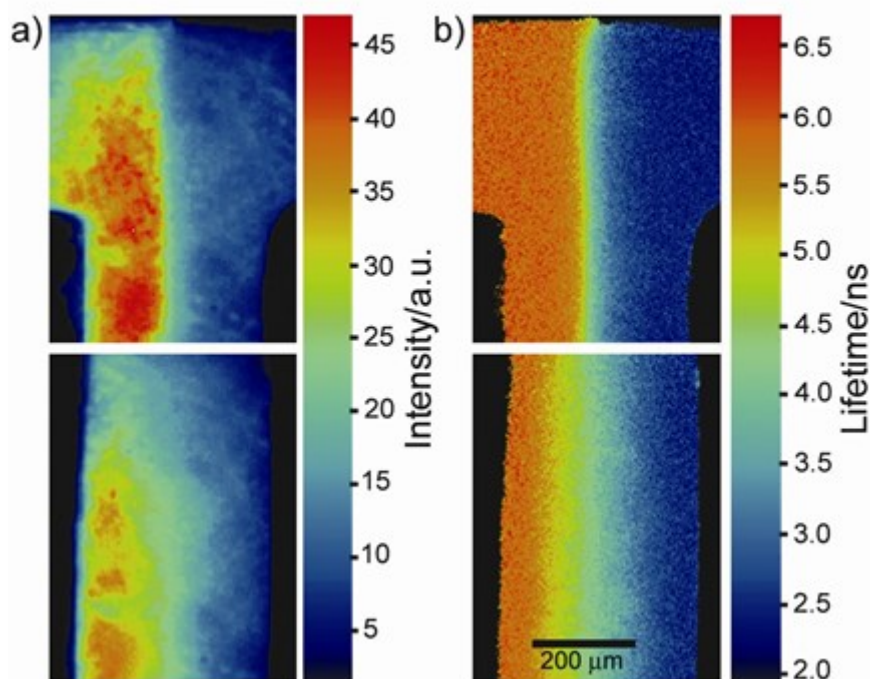
Figure 2. Comparison of fluorescence intensity images (a) and FLIM images (b) for the mixing of solutions of ANS in pure methanol and ANS in a water/methanol mixture (70:30 v/v), using the arrangement shown in Figure 1a. The concentration of ANS in both input solutions was 10^{-3} M and the flow rate was 50 µL/min. For FLIM, the gate width was 600ps, and 46 images were recorded at 500ps intervals. Every image was the average of 5 separate exposures, each of 0.1 s integration time and 50 ms readout time, giving a total acquisition time of *ca.* 35 s. The lifetimes of ANS in pure methanol and the equimolar water-methanol solution at the input to the flow cell are the same as measured by the TCSPC method. The intensity image was constructed by summing the lifetime images, which allows a direct comparison between the time-resolved and intensity-based methods. Using the calibration curve in Figure 1c, the composition of the fluid can be read directly from the FLIM map.

The FLIM technique has been used to monitor mixing as a function of flow rate and flow distance (Figure 3). The compositional variation observed in Figure 3 is indicative of two fluids under laminar flow, as expected. One striking feature of the resultant images is how little mixing occurs in the region where the two input streams meet. Despite being forced together, there is no sign of turbulent mixing. The input streams are well behaved, with no fluctuations in the position of the boundary between them (see Movie S1). Instead, the two streams stay completely separate, except for a narrow mixing region due to diffusion. The overall trend is for the mixing region to broaden as the flow rate decreases, and as the fluids move further downstream, as expected for diffusional mixing. For the fastest flow rate (75 µL/min), regions that are identical in

composition to the input streams persist, even after traveling 1cm down the channel. In contrast, the two fluids have completely mixed at this distance downstream at the slowest flow rate (10 µL/min).
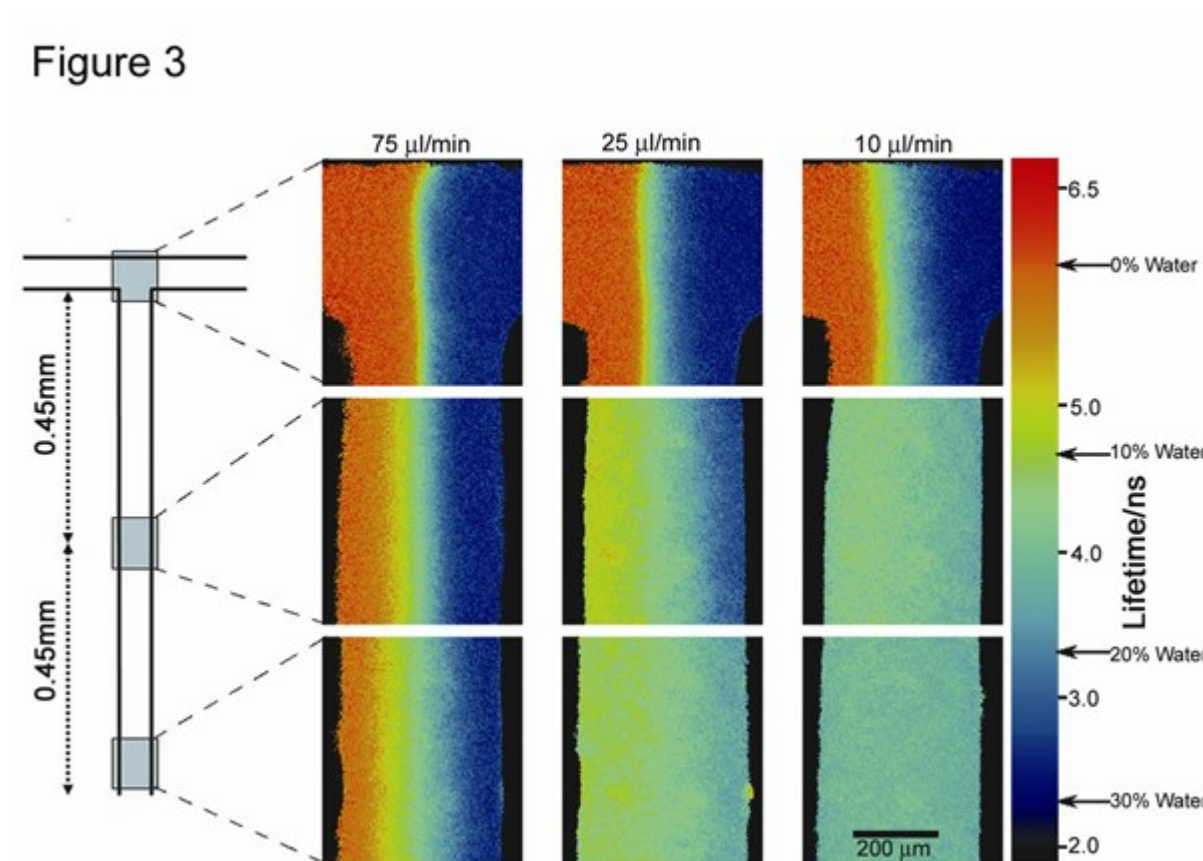

Figure 3. FLIM images for the mixing of solutions of ANS in pure methanol and ANS in a water/methanol mixture (70:30 v/v), showing the spatial dependence of lifetime upon the flow rate and the position within the flow cell. Images were acquired at three positions in the flow cell, and at three flow rates, as indicated. Other experimental parameters are as shown for Figure 2b.

FLIM allows us to monitor mixing with high spatial resolution (Figures 4a and 4b), accurately measuring small changes in the fluid composition in sub-picolitre interrogation volumes. The technique is sensitive enough to reliably detect a *ca.* 2% change in the volume fraction (Figure 4c); this is equivalent to a lifetime change of *ca.* 250 ps, which is a measurement limit set by the temporal width of the detection windows. The compositional resolution could be improved by increasing the time-resolution of fluorescence detection, using photon counting methods. This method is equally applicable to diffusional mixing (the fluorescence lifetime responds to the net diffusion of water molecules across the flow boundary) and mixing by mass transport of fluid, and is, therefore, generally applicable to the evaluation of all types of micromixers. The quantitative

spatial profiles of fluid composition that can be generated by FLIM (Figures 4c and 4d) will be particularly valuable for supporting and guiding theoretical models of fluid flow in microfluidic systems.
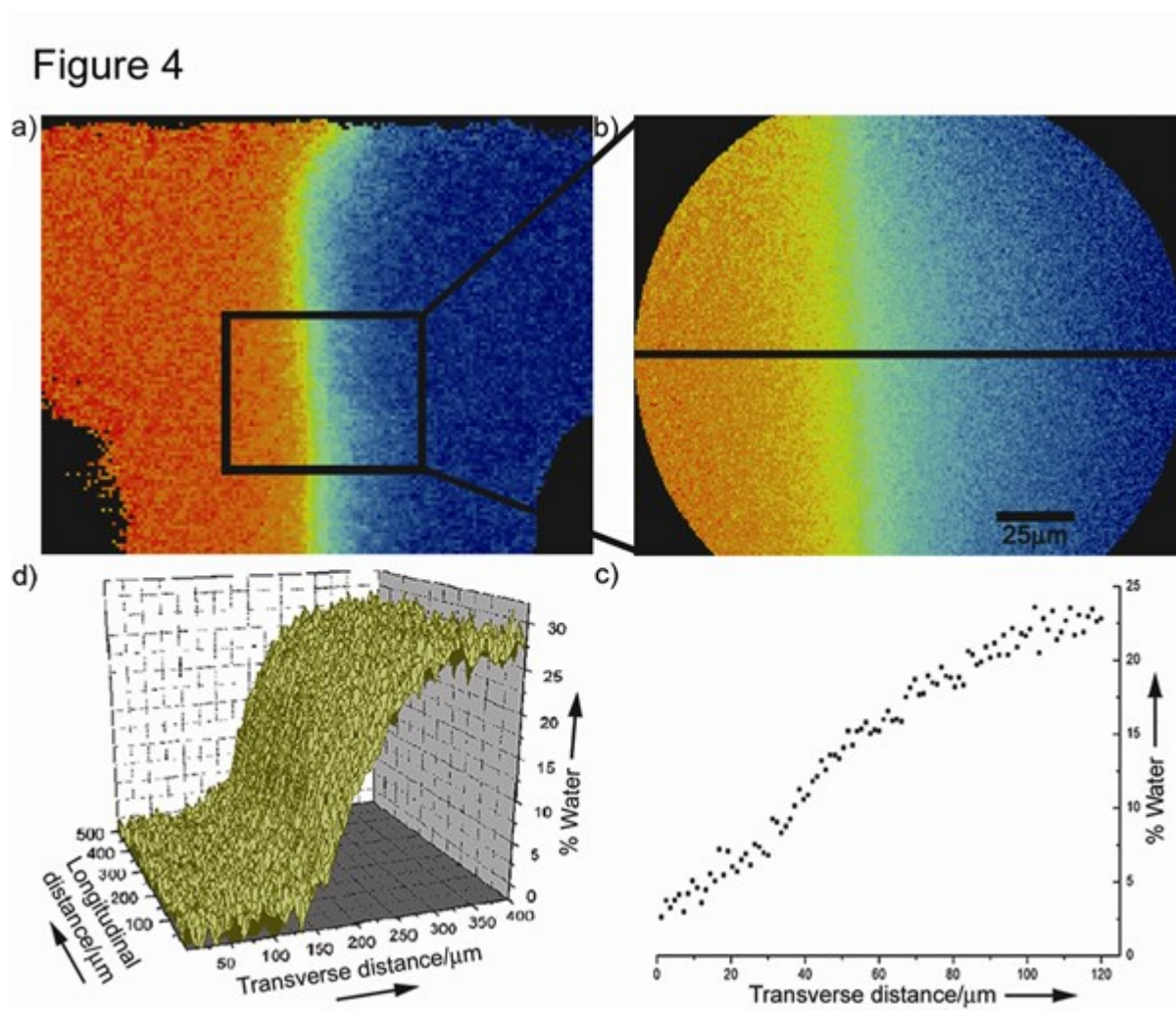
Figure 4. Quantification of mixing using FLIM. (**a**) FLIM image of the mixing of methanol and water/methanol using a 20× objective. The arrangement shown in Figure 1a was used, and the flow rate was 75µl/min. (**b**) Expanded image of the same mixing region using a 100× objective. (**c**) Composition profile along the cross section indicated in Figure 4b. (**d**) Representation of the lifetime data in Figure 4a as a composition surface. Composition values were calculated using the calibration curve in Figure 1c.

The present results demonstrate that widefield FLIM can directly measure the two-dimensional mixing of fluids in microfluidic systems with a level of quantitation that is not available from other methods. It has been shown that intensity-based techniques such as confocal microscopy[13] and optical coherence tomography[23] can provide three-dimensional imaging of microfluidic flows. This is important when the variations in fluid

composition are along the optical axis, since these cannot be resolved by intensity-based widefield methods.[23] Our widefield FLIM technique would, however, detect non-uniform mixing along the optical axis, i.e. the depth axis of the microchannel, since the superposition of a number of layers of different composition along this axis would result in the observation of a multiexponential fluorescence decay, rather than the single exponential decay characteristic of uniform mixing throughout the depth of field. The FLIM approach can be extended to full three-dimensional imaging by using confocal or multiphoton excitation, while still maintaining the attendant benefits of time-resolved detection that have been established here. In this version of the technique, the tightly focused excitation laser beam is rastered across the sample and the fluorescence decay is acquired point-by-point, using time-correlated single photon counting. The use of multiphoton excitation would also enhance imaging penetration through strongly absorbing or scattering fluids or structures.

The mixed solvent system used in the present work, in conjunction with the ANS probe, was devised purely as a measurement tool for the generic study of micromixing, and was not intended to relate to any specific applications of lab-on-a-chip systems. Our approach is, however, generally applicable to any solvent system, as long as there is a change in molecular environment upon mixing that results in variation in the fluorescence lifetime of an appropriate probe. For example, mixing of aqueous solutions could be studied by using streams of different pH that incorporate a pH-sensitive dye, such as a seminaphthorhodafluor (SNARF) probe. Alternatively, streams containing different concentrations of a collisional quencher, such as iodide, could be used. In view of the flexibility of this approach, we anticipate that FLIM will become an essential tool in the design, modeling and evaluation of microfluidic systems.

Experimental Section

All measurements were made with the ammonium salt of ANS (Fluka, used as received). The methanol and water used in this study were HPLC grade (Fisher Scientific) and were used as received. Solutions of ANS (*ca.* 1×10^{-3}M) were stored in the dark, and the lifetime of ANS fluorescence at room temperature was used as a routine check of sample purity after storage. No emission could be detected from the solvents under the instrumental conditions employed. Time-resolved fluorescence spectroscopy was performed using the technique of time correlated single photon counting as described previously.[22]

The microfluidic cell was fabricated from Perspex with the 'T' shaped channel milled out to a depth of 0.2 mm using a 0.4 mm diameter end mill (Drill Service Ltd). The 3 inlet/outlet holes were drilled 1.6 mm in diameter and fitted with polypropylene tubing. The cell was sealed by gluing (Norland Optical Adhesive No. 61) a coverglass over the channels, and was attached to syringes using silicone tubing. The flow of fluids from the syringes was controlled by a syringe pump (Univentor 802, Univentor Ltd.).

For FLIM, frequency-doubled light from a mode-locked Ti-Sapphire laser at 400 nm, with 4.75 MHz repetition rate, was expanded, collimated and directed into a Nikon TE300 inverted microscope operating in an epifluorescence configuration. This excitation light was reflected from a dichroic filter (DM430, Nikon) and focused onto the microfluidic flow cell using either 20× (PA, NA=0.75, Nikon) or 100× (Ph3, NA=1.3, oil immersion, Nikon) objectives. The laser power incident on the flow cell was typically around 100 μW. The resultant fluorescence was collected through the same objective, passed through a 515-555 nm barrier filter (Nikon) and imaged onto a Picostar HR-12QE gated intensified CCD camera system (LaVision GMBH, Berlin). The excitation beam was split, and one portion was used to trigger a fast photodiode. The photodiode output was passed through a constant fraction discriminator (CF4000, Ortec), and used as the trigger signal for the Picostar system. The experiments described herein were recorded with a 600 ps gate width, which was measured by detecting laser light reflected from a mirror (the minimum gate width for this camera is 200 ps). The intensifier gate was delayed relative to the laser trigger signal using a DEL150 picosecond delay module (Becker and Hickl). The 12-bit CCD camera is a progressive scan interline sensor, with 1370 (H) by 1040 (V) pixels (pixel size is 6.45 μm × 6.45 μm). Images were the average of 5 separate exposures, and were recorded in steps of 500 ps over a 23 ns range, and employed 4 × 4 hardware binning. The integration time for each image was 0.1 ms, with 0.05 ms readout time, giving a total acquisition time of approximately 35s. The excitation intensity was adjusted to give a peak intensity of between 3000 and 4000 counts in the brightest image, which corresponds with the start of the fluorescence decay. The background signal of *ca.* 50 counts was subtracted from each image. The Picostar system and delay card were controlled, and the data were analyzed, using DaVis 6.2 software running the Picostar DaVis module. The peak of the fluorescence intensity was found in the fourth image of the image series. To ensure that the instrument response did not interfere with the fitting, the first five images were not used for analysis. The sixth image, which was 1 ns after the peak, and the subsequent images were analyzed, allowing a decay curve to be constructed for each pixel. Pixels with low counts in the first analyzed image (typically 700 counts) were removed at this stage. Each of these curves was then fitted to a single exponential decay. A lifetime map was produced by assigning a color on a 16-bit pseudocolor scale to each of the fitted lifetimes, and these were displayed over a range of 2-6.8 ns.

References

[1] T. Vilkner, D. Janasek, A. Manz, *Anal. Chem.* **2004**, *76*, 3373.

[2] A. Hibara, M. Nonaka, M. Tokeshi, T. Kitamori, *J. Am. Chem. Soc.* **2003**, *125*, 14954.

[3] S. Xu, Z. Nie, M. Seo, P. Lewis, E. Kumacheva, H. A. Stone, P. Garstecki, D. B.   Weibel, I. Gitlin, G. M. Whitesides, *Angew. Chem.* **2005**, *117*, 734; *Angew. Chem.   Int. Ed.* **2005**, *44*, 724.

[4] H. Song, J. D. Tice, and R. F. Ismagilov, *Angew. Chem* **2003**, *115*, 792; *Angew.   Chem. Int. Ed.* **2003**, *42*, 768.

[5] P. D. I. Fletcher , S.J. Haswell , E. Pombo-Villar , B. H. Warrington, P. Watts, S.   Y. F. Wong, X. Zhang, *Tetrahedron* **2002**, *58*, 4735.

[6] M. U. Kopp, A. J. de Mello, A. Manz, *Science* **1998**, *280*, 1046.

[7] D. R. Reyes, D. Iossifidis, P.-A. Auroux, A. Manz, *Anal. Chem.* **2002**, *74*, 2623.

[8] B. Zhao, J. S. Moore, D. J. Beebe, *Science* **2001**, *291*, 1023.

[9] B. H. Weigl, P. Yager, *Science* **1999**, *283*, 346.

[10] H. Chen, J.-C. Meiners, *Appl. Phys. Lett.* **2004**, *84*, 2193.

[11] L.E. Locascio, *Anal. Bioanal. Chem.***2004**, *379*, 325

[12] T.J. Johnson, D. Ross, L.E. Locascio, *Anal. Chem.***2002**, *74*, 45.

[13] A. D. Stroock, S. K. W. Dertinger, A. Ajdari, I. Mezić, H. A. Stone, G. M.   Whitesides, *Science* **2002**, *295*, 647.

[14] J. M. Ottino, S. Wiggins, *Science* **2004**, *305*, 485.

[15] F. Schönfeld, V. Hessel, C. Hofmann, *Lab Chip* **2004**, *4*, 65.

[16] M. S. Munson, P. Yager, *Anal. Chim. Acta* **2004**, *507*, 63.

[17] P. J. A. Kenis, R. F. Ismagilov, G. M. Whitesides, *Science* **1999**, *285*, 83.

[18] R. M. Clegg, O. Holub, C. Gohlke, *Methods Enzymol.* **2003**, *360*, 509.

[19] F. G. Haj, P. J. Verveer, A. Squire, B. G. Neel, P. I. H. Bastiaens, *Science* **2002**,   *295*, 1708.

[20] T. W. J. Gadella Jr., T. M. Jovin, *J. Cell. Biol.* **1995**, *129*, 1543.

[21] J. R. Lakowicz, H. Szmacinski, K. Nowaczyk, M. L. Johnson, *Proc. Natl. Acad. Sci. USA* **1992**, *89*, 1271.

[22] L. Dougan, J. Crain, H. Vass, S. W. Magennis, *J. Fluoresc.* **2004**, *14*, 91.

[23] C. Xi, D. L. Marks, D. S. Parikh, L. Raskin, S. A. Boppart, *Proc. Natl. Acad. Sci. USA* **2004**, *101*, 7516.